Additive Manufactured Ultra-Fine Lattice Structures for Propulsion Catalysts

Omar R. Mireles[1], Zachary Jones[2], and Omar Rodriguez[3]
NASA Marshall Space Flight Center, Huntsville, AL, 35812, USA

Maryna Ienina[4]
EOS North America, Pflugerville, TX, 78660, USA

Traditional mono-propulsion catalysts consist of coated ceramic or graphite foams that possess anisotropic mechanical and fluid properties limiting design, cost, availability, and operational use. Ultra-fine lattice structures are repeating unit cells with ligament thickness as small as 100 µm produced via Additive manufacture (AM). These lattice structures have the potential to replace coated foams used in a mono-propellant system catalysts. AM ultra-fine lattice structures are designed to mimic the operational intent of coated foams but with improved design flexibility, compressive strength, and flow behavior printed from into a single part directly from the preferred platinum metal alloy. The investigation objective was to conduct feasibility studies of AM ultra-fine lattice structures capable of replacing coated foams with superior functionality. NASA MSFC identified desired lattice characteristics and created designs while EOS developed optimized laser powder bed fusion AM parameters to manufacture Ti6Al4V and tungsten specimens. Optimized designs, computational tools, AM parameters, and post-process methods were developed. Specimens underwent x-ray micro-focus CT, metallographic inspection, compression testing, and flow testing. Results demonstrate that AM ultra-fine lattices improved geometric and performance repeatability with the potential for significantly increased availability while decreasing cost and lead time.

I. Nomenclature

a	=	unit cell
AM	=	additive manufacture
BO	=	beam offset
CT	=	computer tomography
D	=	hatch spacing
DOE	=	design of experiment
E_a	=	area energy distribution
EDM	=	electro-discharge machining
E_v	=	energy density
GN_2	=	gaseous nitrogen
K_v	=	flow coefficient
L-PBF	=	laser powder bed fusion
mm	=	millimeter
MPa	=	mega-Pascal
MSFC	=	Marshall Space Flight Center
P	=	power

[1] Additive Manufacture R&D Engineer, In-Space Propulsion Branch.
[2] Additive Manufacture Engineer, Additive Manufacture Branch.
[3] Materials Engineer, Materials Characterization Branch.
[4] Application Engineer, Metals Group.

Q	=	volumetric flow rate
PSIA	=	pounds per square inch absolute
SEM	=	scanning electron microscopy
SiC	=	silicon carbide
SS	=	stainless steel
t	=	layer thickness
T	=	temperature
TRL	=	test readiness level
UTEP	=	University of Texas, El Paso
v	=	laser scan speed
V	=	volume
W	=	tungsten
Z	=	build direction
ΔP	=	pressure drop
γ	=	specific gravity
ρ	=	density
μm	=	micrometer
μ-CT	=	micro-focus computer tomography
%RD	=	percent relative density

II. Introduction

NASA Marshall Space Flight Center (MSFC) has been maturing the application of additive manufacture (AM) for improved performance and cost reduction of propulsion systems. Traditional mono-propulsion catalysts consist of coated ceramic or graphite foams with thousands of irregular pores with varying size and distribution [1]. These foams exhibit anisotropic mechanical properties, inconsistent fluid flow behavior, and due to manufacturing limitations constrain design, cost, availability, and operational use. Foams are coated with a refractory platinum metal, which utilize well-known processes; however, have resulted in spatially non-uniform deposition, particularly in the foam interior. These catalysts are produced by a limited number of suppliers that constrain availability and cost. In addition, mechanical and fluid flow properties can vary widely depending on the porous substrate manufacture method and the subsequent coating method utilized to arrive at a final part [2]. During installation these coated foams are highly susceptible to damage by compressive press fitting into the reaction chamber. What is required is another method to manufacture mono-propellant thruster catalyst materials with improvements in properties, availability, and cost. Ultra-fine lattice structures are repeating unit cells with ligament thickness as small as 100 μm produced through AM. These lattice structures have the potential to replace coated ceramic of graphite foam catalysts. AM lattice structures offer greater control over structure topology allowing for customized percent relative density (%RD), which has is used to control mechanical and fluid flow properties [3]. These AM lattice structures are designed to mimic the operational intent of coated foams but with unconstrained design flexibility, improved compressive strength with fluid flow optimization printed into a single part directly from the preferred refractory platinum metal. Although the work described here was conducted for mono-propellant systems such as green propellant thruster catalysts, the same lattice structure technology can be applied in gas or liquid permeable rigid materials, evaporative film cooling heat exchangers, filtering, etc. [3]. AM also enables the ability to include lattice structures integral to the final part followed by coating, potentially eliminating the need for installation in an assembly as done with traditional methods.

III. Methodology

The objective of this investigation was to conduct feasibility studies of the ability of AM to produce ultra-fine lattice structures capable of replacing metallic or graphite foams. Methods were to leveraging existing investments in AM technology develop, partnerships, and infrastructure to minimize cost. From a property perspective the AM lattice structure material must exhibit behavior similar to that of existing porous foams or gas/liquid permeable material but with improved control over geometric repeatability that could possibly yield more reliable fluid, mechanical, and chemical reaction properties. The project was divided into several phases of development in order iteratively mature the process as lessons are learned. The phases included lattice structure design, AM parameter development, AM ultra-fine lattice specimen production, microstructural characterization, non-destructive evaluation, mechanical testing, and flow testing.

A. Lattice Structure Design

MSFC identified the desired lattice characteristics by characterizing porous foam samples as shown in figure 1 in order to design an AM lattice topology. Target pore size, strut thickness, pressure drop range, and compressive strength requirements were determined and used to guide the lattice topology selection and design process.

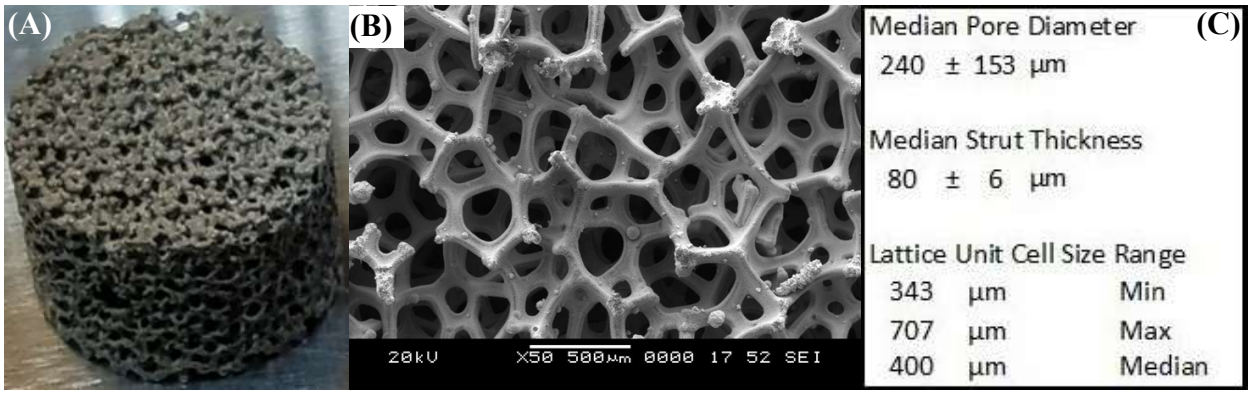

Fig. 1 Iridium/Rhenium coated SiC foam catalyst (A), graphite foam SEM micrograph at 50x (B) and AM lattice design target specifications (C).

Initial lattice topology candidates were selected from the Materialise Magics structures library and printed from tungsten (W) on an EOS M100 at MSFC as shown in figure 2. Specimens were found to print reliably with no difficulties removing un-melted powder; however, as the unit cell size (*a*) decreased the standard topologies became increasingly computationally expensive and did not reliably yield the desired pore size and strut thickness specifications. Therefore, additional topologies would have to be explored or custom-designed.

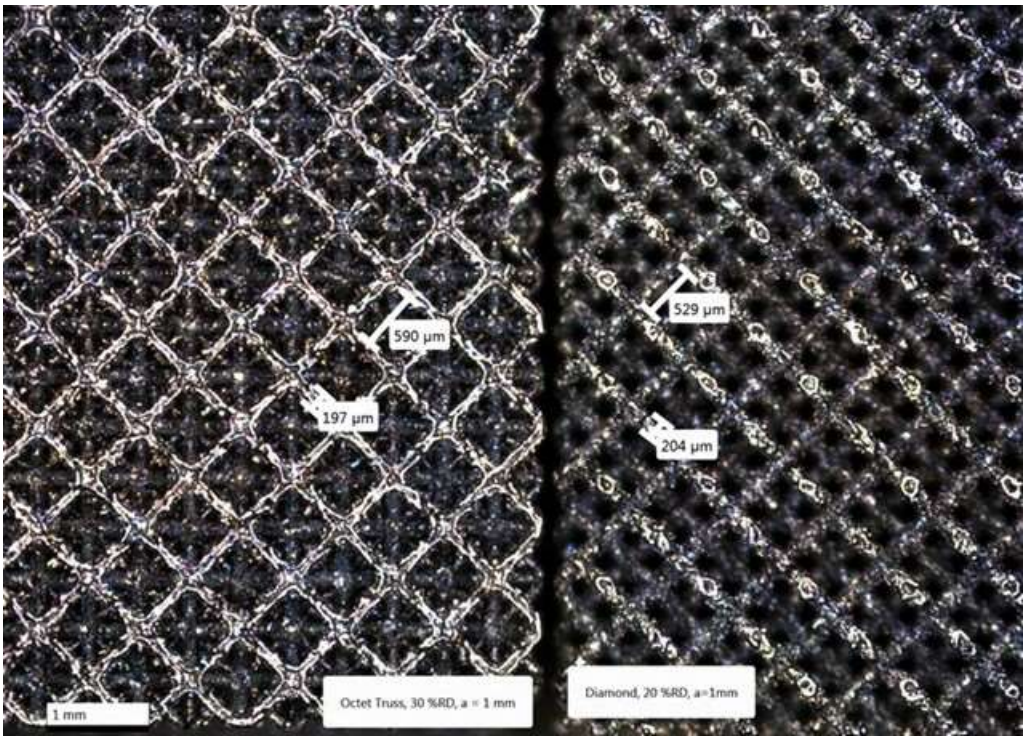

Fig. 2 Octet Truss-30 %RD (left), Diamond-20 %RD (right). W specimens, *a* = 1 mm (100x).

Topologies from the Autodesk Netfabb Ultimate lattice library were explored and Netfabb was used to design custom lattice topologies that would meet characteristic requirements and are illustrated in Figure 3.

Name	Image	Hatch lines in EOSPrint	Geometry	Exposure Type
Hexa_Profile_0m	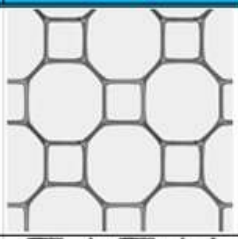		Volume	Support
Penta_Cube_0m	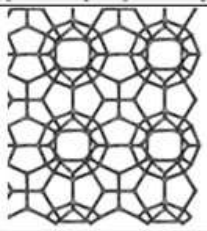		Support	Support
Lattice-04_40µm_0m	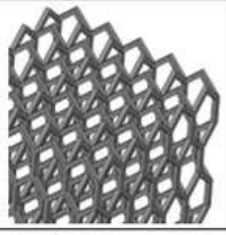		Volume	Support
Lattice-04_60µm_0m			Volume	Support
Lattice-04_80µm_0m	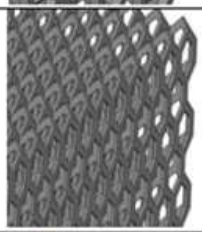	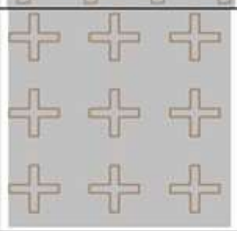	Volume	Support
Lattice-04_ 70µm_surface_0m	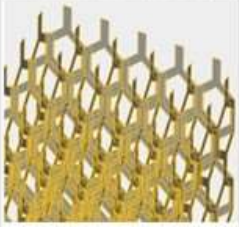		Surface	Support
Grasshopper	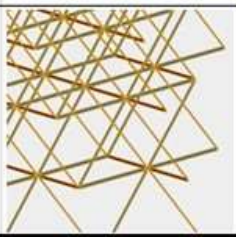	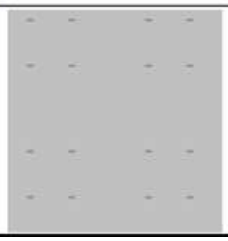	Surface	Support

Fig. 3 Standard library and custom ultra-fine lattice topology candidates.

B. Build Parameter Development and Specimen Production

Laser Powder Bed Fusion (L-PBF) was selected over other AM methods due to the small laser focus diameter and that powder adjacent to the melt pool does not sinter to an excessive degree to prevent powder removal after printing. A design of experiments (DOE) was conducted by EOS to develop L-PBF build parameters. Volumetric energy density (J/mm^3) is optimized for the core or infill scan strategy, which is determined using equation (1).

$$E_v = \frac{P}{vDt} \tag{1}$$

P is the laser power units of W, v is the laser scan speed in mm/s, D is the hatch distance in mm, and t is the layer thickness in mm. Single line scan strategy used for support structures and contours, where E_a or the area energy density (J/mm^2) is optimized using equation (2).

$$E_a = \frac{P}{vt} \tag{2}$$

Three trials defined geometry, while 12 trials were used to define optimal energy input, exposure strategy (*D*, contour, as vector lines) and beam offset (*BO*). Optimal processing parameters for the laser and scanning were defined by test matrix that focuses on the energy density in the powder bed. The energy input variable can be quantitatively changed based on the commanded laser power and the speed at which the laser scanner moves the beam in the XY dimensions. For example, a high laser power and low speed might result in an excessive energy input and subsequently melt too much material, resulting in thicker lattice struts making the pores too small and powder difficult to remove. Conversely, a low laser power and high speed will not impart sufficient energy to melt the material. Once the complex lattice structures were successfully manufactured the process will reliably reproduce the same specimens with a high degree of repeatable quality and more predictable performance.

Parameter development was first conducted for Ti6Al4V then for W to act as low-cost surrogate materials in order to develop the process before attempting expensive refractory platinum metals such as Rhenium or Iridium. An EOS M100 L-PBF platform has a nominal laser focus diameter of 40 µm, which allows for fine geometric features to be produced between 1.8-2 times the laser focus diameter. Low resolution optical microscopy found that the M100 was able to produce lattice structure unit cells with strut diameter within the goal of approximately 100 µm. Additional specimens were printed on the MSFC EOS M100 from W using the same build parameters in order to increase the number of specimens needed for microstructural, mechanical and fluid flow characterization.

Fig. 4 EOS M100 L-PBF platform printing W lattice specimens.

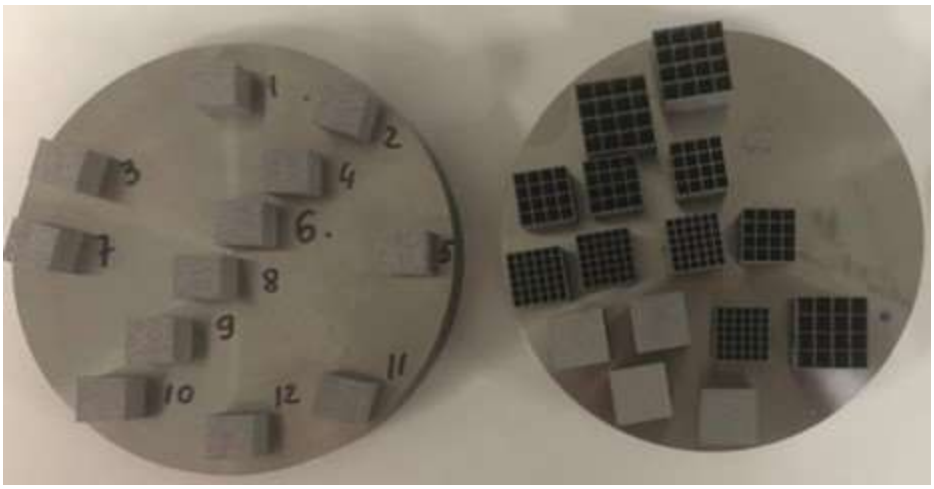

Fig. 5 Ti6Al4V cube specimen print trial DOE 1.

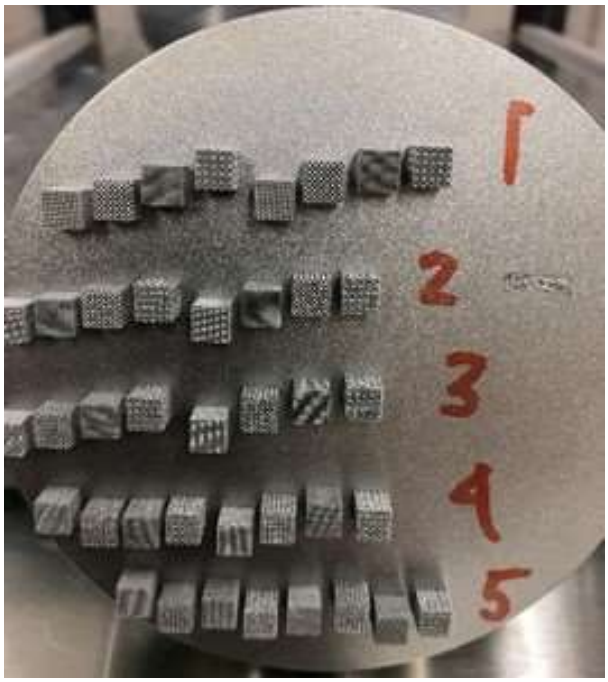

Fig. 6 W cube specimen print trial DOE 6.

C. Lattice Specimen Post-Processing

Lattice specimens underwent powder removal through a combination of mechanical agitation, compressed argon, and vacuum to minimize the amount of un-melted powder trapped within the lattice cell volumes. Next, the lattice specimens were removed from the build plate using wire-EDM, water rinsed, and air dried. After plate removal specimens underwent a more thorough powder removal process by flowing compressed air through the specimens in parallel, perpendicular, and transverse to the build direction in a fume hood. The process was repeated until no particles were observed to be removed from the specimens. Specimens were then sonicated in deionized water for 30 minutes, with specimens rotated specimens 90° every 10 minutes. After water sonication the specimens were dried with compressed air. The specimens were then sonicated in isopropyl alcohol for 30 minutes with the same rotation schedule then dried with compressed air. It was observed that powder continued to be liberated from the specimens in both water and sonication steps and the number of sonication cycles was repeated as required until little to no powder was observed to be emitted from the specimens. Finally, the lattice specimens were stored in a desiccator for 24 hours prior to subsequent evaluation.

D. Microstructural Characterization

Optical microscopy was conducted at MSFC to determine geometric accuracy of ultra-fine lattice structures, evaluate the as-built surface morphology, and determine the amount of trapped powder within the pores. Ti6Al4V specimens exhibit a substantial amount loosely adhered un-melted powder particles to the as-built surface, which is common for L-PBF produced components as shown in figure 7A. Specimens were sectioned, mounted, ground, and polished in order to evaluate the interior. As shown in figure 7B the lattice topology is retained, although there are still trapped powder within the pores and some strut cracking. It was found that the metallographic preparation process could induce fractures in the struts, when compared to non-destructive evaluation methods later in this paper. The amount of powder adhering to W specimens was less than in Ti6Al4V but was still evident as shown in figures 8 through 11. W specimen struts exhibited smoother surface finish. It must be noted that the powder particle size distribution for W powder was smaller than for Ti6Al4V, which is one of the factors used to improve surface finish of L-PBF components. Surface adherent powder could be potentially beneficial if the ultra-fine lattice is printed from catalytic refractory platinum metal due to an increased surface area that in-part drives the associated reaction kinetics when exposed to flowing propellant. It is likely the adherent powder would react and erode away during the first green run hot fire test but that has yet to be confirmed. A smoother surface finish may be desired for powder removal and lower fluid pressure drop across the catalyst. From a mechanical property perspective a rougher surface finish can decrease fatigue life; however, fatigue was not one of the dominant failure mechanisms identified during thruster operation. Additional secondary processes such as chemical etching may be required to remove residual un-melted powder to improve surface finish if needed.

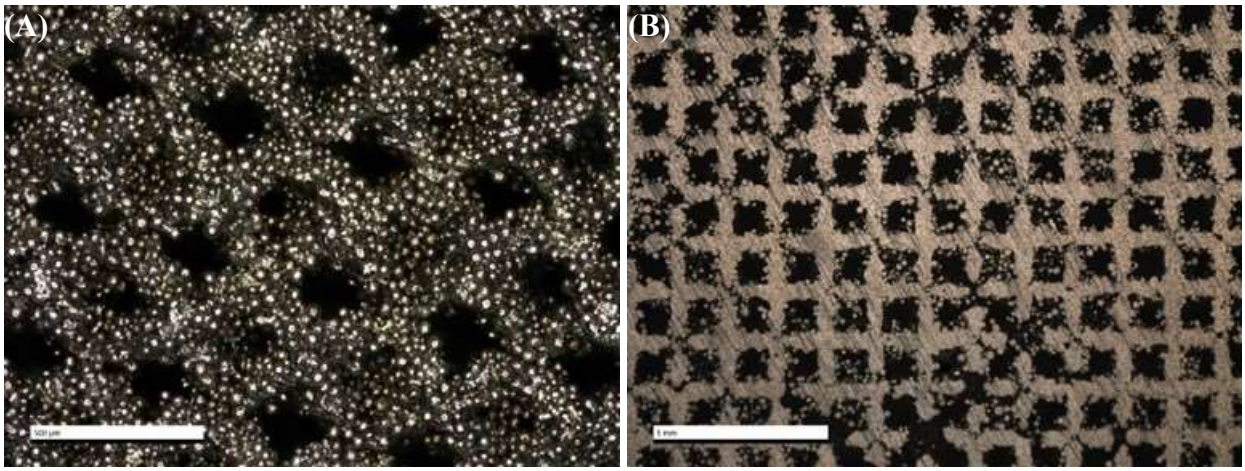

Fig. 7 Optical micrograph of Ti6Al4V Grasshopper lattice #19 as-built at 200x (A) and ground #16 at 100x (B).

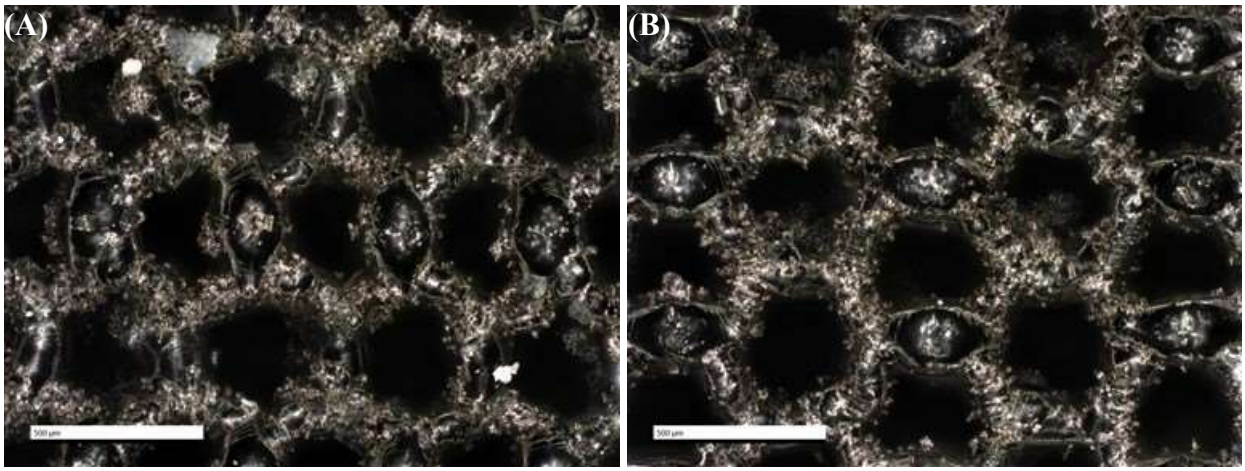

Fig. 8 Optical micrograph of Hexa Profile W lattice, as-built in XY (A) and XZ (B) at 200x.

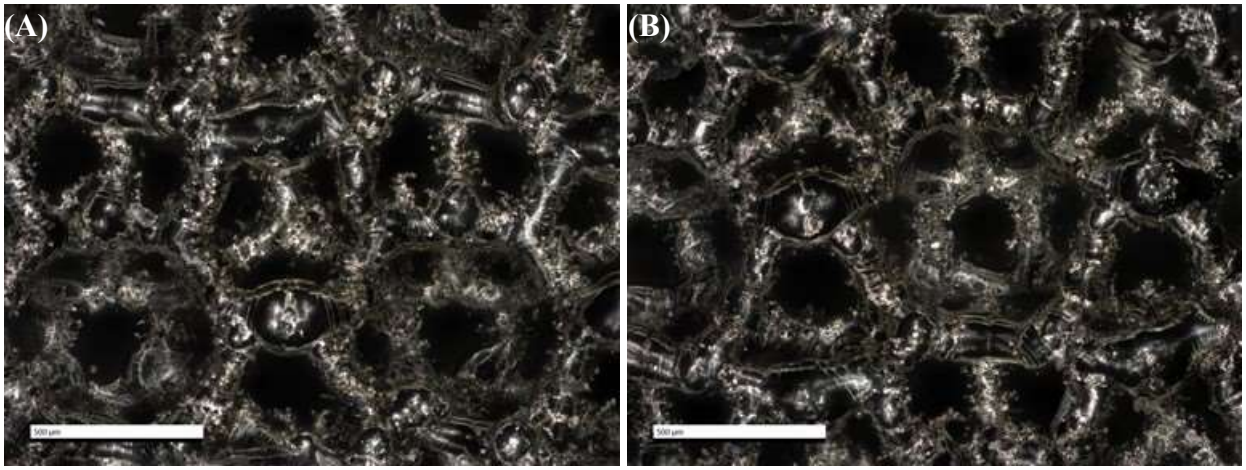

Fig. 9 Optical micrograph of Penta Cube W lattice, as-built in XY (A) and XZ (B) at 200x.

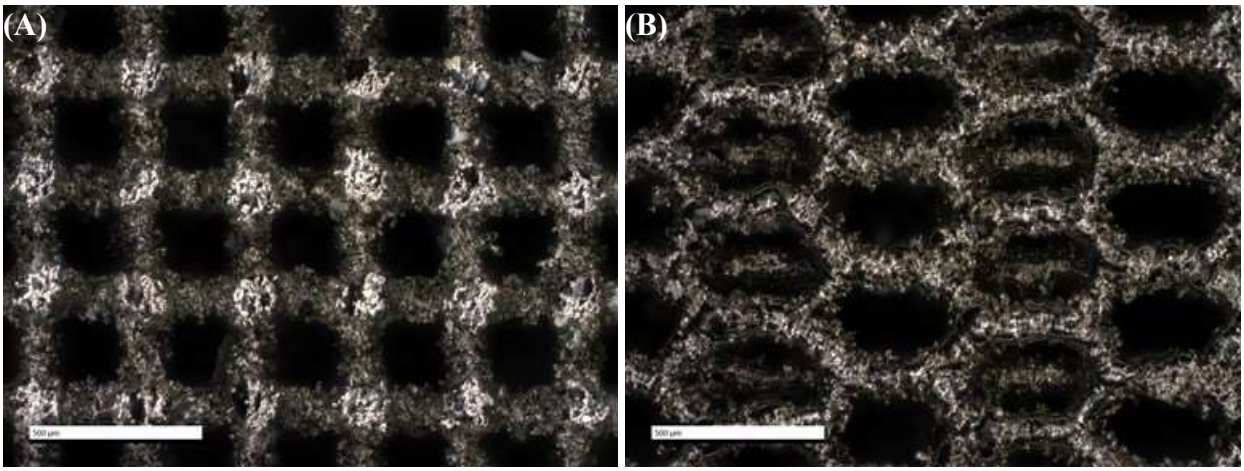

Fig. 10 Optical micrograph of 40 µm size surface W lattice, as-built in XY (A) and XZ (A) at 200x.

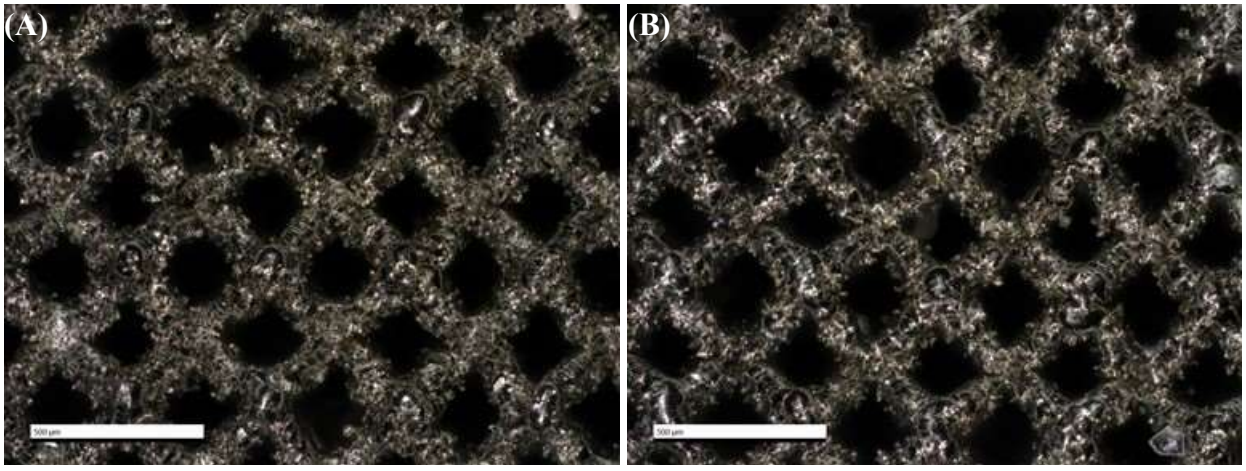

Fig. 11 Optical micrograph of Grass Hopper W lattice, as-built in XY (A) and XZ (B) at 200x.

Optical micrographs of as-built W DOE 6 lattice specimens were obtained in the XY and XZ planes as a function of the L-PBF parameter energy density. Image processing was used to several measurements of each lattice structure geometric feature. These measurements were then used to derive the average strut thickness, average pore diameter (inter-strut cell size), and average unit cell size and associated standard deviations as function of energy density as shown in Figures 12 and 13.

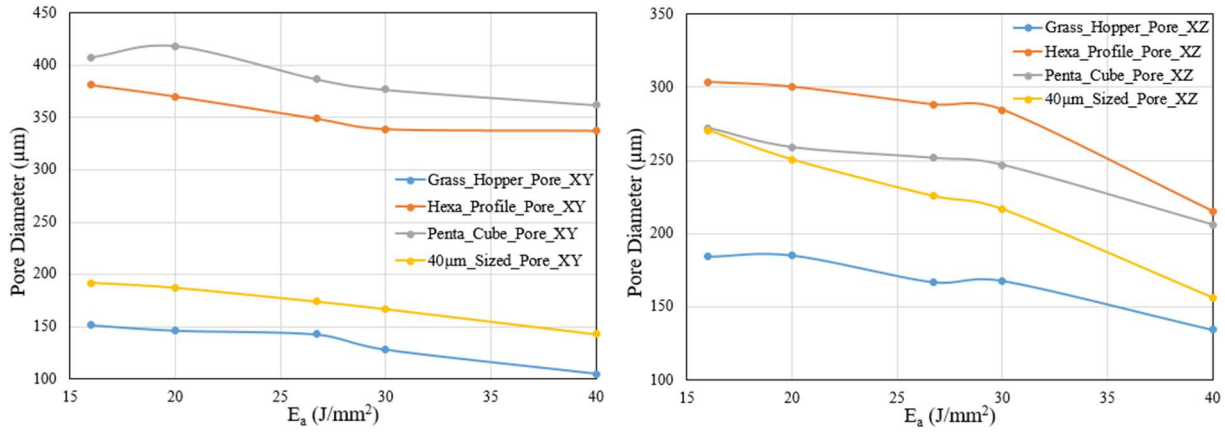

Fig. 12 W DOE 6 pore diameter vs. E_a based on as-built optical microscopy measurements.

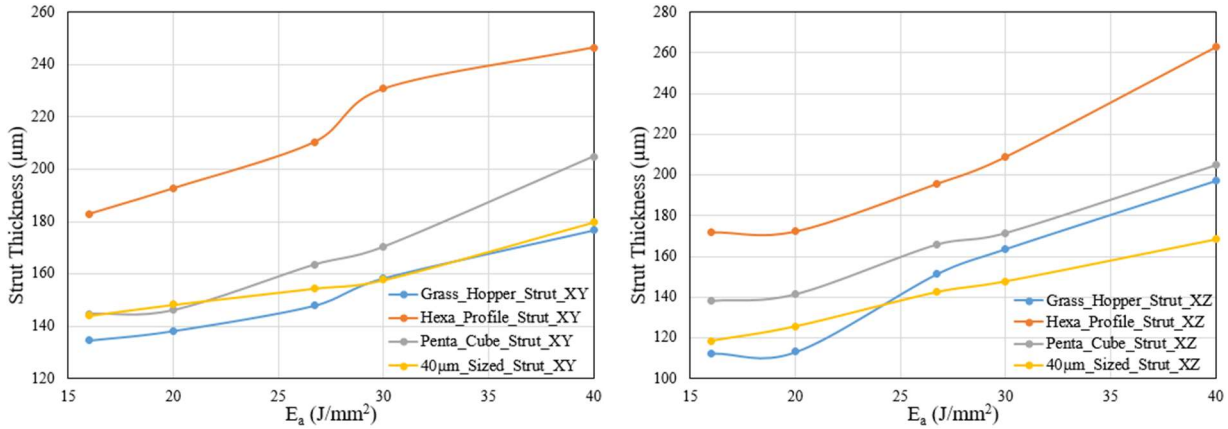

Fig. 13 W DOE 6 strut thickness vs. E_a based on as-built optical microscopy measurements.

A higher energy density generates a larger melt pool, which then results in larger strut thickness. It can be observed in Figure 13 that strut thickness is indeed proportional energy density. Conversely, the pore size is inversely proportional to the energy density. The unit cell size varied somewhat as a function of the energy density and can likely be attributed to either measurement error or residual stress induced distortion. In the case of the lattice topologies, the pore and strut sizes remained varied predictably with topology type, even with when considering change of energy density. The pore size target range was 87 – 393 um and the smallest pore range in XY is Grass Hopper from 106.7 – 157.6 ± 6.7 µm with the largest being Penta Cube from 362.2 – 407.5 ± 8.8 µm. The smallest pore range in XZ is Grass Hopper from 134.4 – 185.5 ± 17.8 µm with the largest being Penta Cube from 362.2 – 407.5 ± 8.8 µm. The majority of the pore sizes are within the target range and can be tailored for pressure drop requirements using specific build parameters. The strut thickness target range was 74 – 86 µm. The smallest strut range in XY is Grass Hopper 134.6 – 176.7 ± µm with the largest being Hexa Profile from 183.0 – 246.4 ± 7.5 µm. The smallest strut in XZ is 40 µm Sized Surface from 118.4 – 168.6 ± 11.9 µm with the largest being Hexa Profile from 172.0 – 262.8 ± 10.8 µm. Strut thickness exceed the desired target range varying between 2x to 4x that of nominal. It can be expected that although thicker struts with a corresponding small pore size may be deleterious to flow properties, this also implies such topologies will exhibit stronger mechanical properties. Although optical micrographs provided a degree of geometric measurement, their result is highly localized and unable to provide insight on the spatial distribution of these geometric features. For that reason, non-destructive methods are now discussed.

E. Geometric Non-Destructive Examination

3D Engineering Solutions was contracted to inspect a series of ultra-fine lattice specimens using x-ray micro-computer tomography (µ-CT). The high spatial resolution provided by µ-CT was able to discern fine geometric features such as changes in strut thickness and cell volume (inter-strut pore size) throughout the entire specimen as shown in Figure 14. In addition, un-melted powder trapped within cell volumes that was not removed during post-print cleaning was found and appear as a lower density regions in the scan images as shown in Figure 14C. Ti6Al4V and W CT lattice specimens were provided and included Hexa Cube (#9), Penta Cube (#15), 40 µm Sized-Surface (#29), and 40 µm Sized-Surface (#33). Ti6Al4V has a relatively low effective atomic number with low radio-opacity, meaning that a sufficient x-ray flux can penetrate into the part and to the detector to yield a sufficiently high signal-to-nose ratio that allow for images to be resolved with adequate resolution [4], [5].

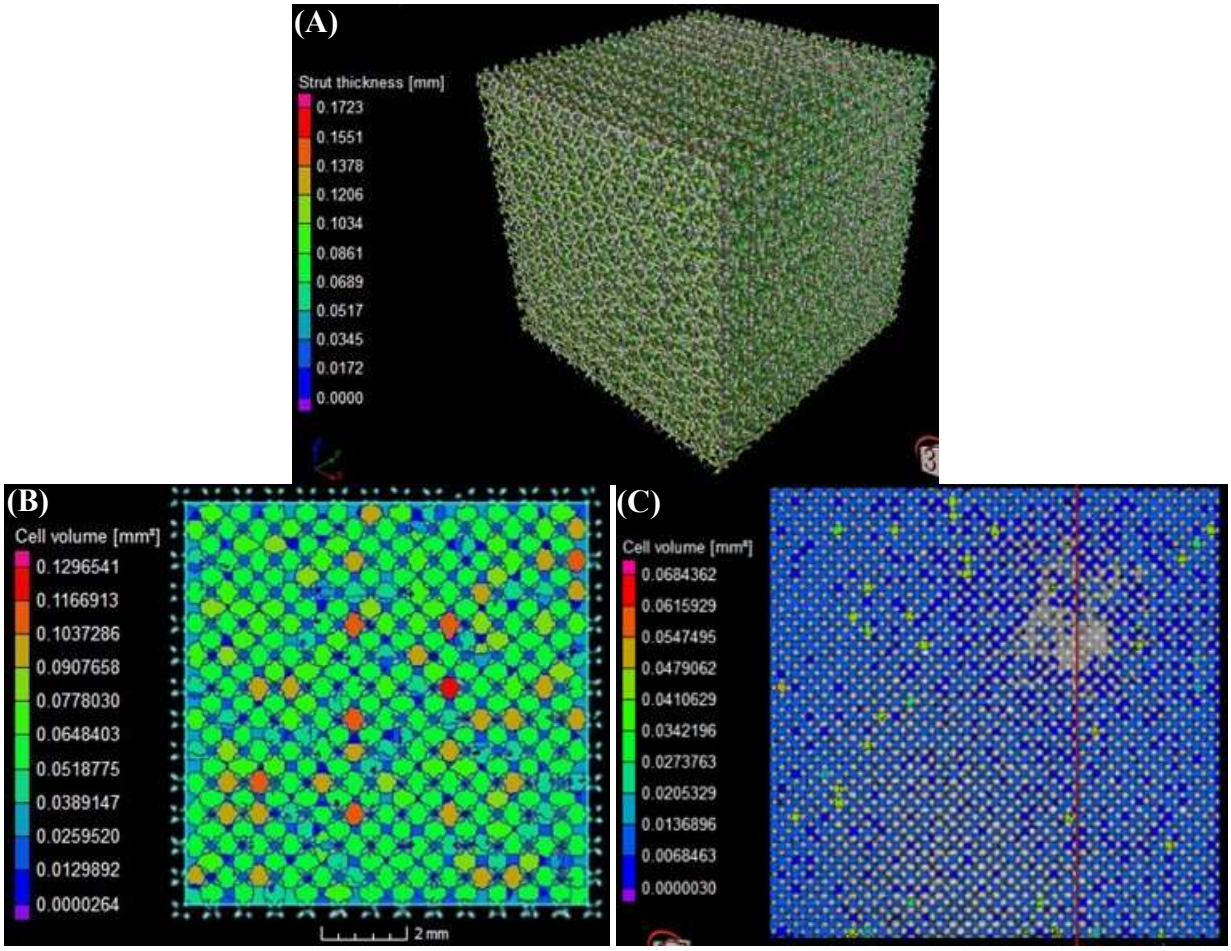

Fig. 14 µ-CT images of Ti6Al4V ultra-fine lattice specimen strut thickness (A), cell volume (B) and trapped powder (C). Courtesy 3D Engineering Solutions.

The Ti6Al4V scans show spatial variations in strut thickness, cell volume, and trapped powder within cell volumes. Ti6Al4V specimen scan images yielded excellent specimen geometric feature resolution, which is then compared to the CAD file in order to determine variation between as-designed and as-printed conditions. As seen with optical microscopy the strut diameters are on the upper limit of the design specification, which also results in reduced pore diameter and cell volume. As expected µ-CT was unable to resolve useful images for inspection of the W specimens due to having a high atomic number and associated high radio-opacity resulting in high scatter, low penetration depth, and poor signal-to-noise ratio. It must be noted that although µ-CT is very powerful tool, it is not necessarily practical for routine inspection of intricate or large parts in high production rate scenario due to the long scan times, large data files, and cost. µ-CT should be utilized to characterize geometric changes in the initial production process order to compensate designs for subsequent production without utilizing these inspection methods.

F. Mechanical Testing

The compressive quasi-static (0.001 ε^{-1}) behavior of ultra-lattice cube specimens (10x10x10 mm) was characterized using a Psylotech meso-scale load frame equipped with a 10kN load cell. Lattice specimens were tested with its loading axis parallel to the build axis. A self-aligning loading block ensured that the load was distributed as uniformly as possible during the entire test. Deformation was recorded by the crosshead displacement. The engineering stress and strain of the loaded lattice specimens were obtained by dividing the reaction force by the original cross-sectional area and the displacement by the un-deformed height of the specimens respectively. Consequently, the flow stress curves depicted by Figures 15 and 16 are a true representation of the lattice structure. It must be noted that the flow stress data illustrated in these figures has been truncated to the first recorded localized fracture on struts or nodes, which was chosen as a criteria for material failure.

As expected, strength and ductility showed a dependence not only on the specific lattice topology but also on the build parameters used to generate the specimens. As stated by a previous study, structural geometry should have a major role in the mechanical response since different struts may experience different deformation modes including tension, compression, bending or a combination of these modes [6]. Similarly, the influence of AM build parameters on the mechanical performance of components has been well documented. Figure 15 groups the compressive behavior of each lattice topology type as a function of build energy density.

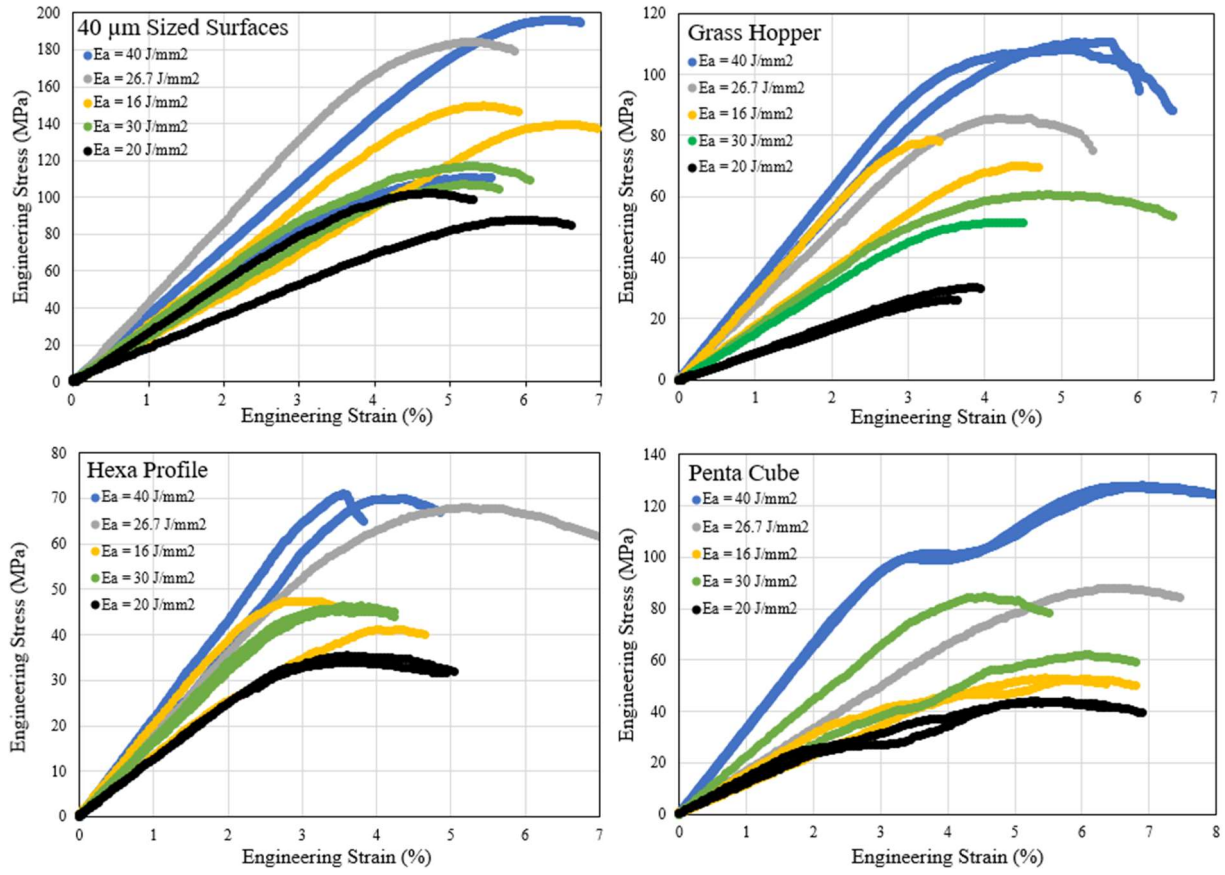

Fig. 15 Compressive strength of as-built AM W lattice structures where topology is constant and E_a varied.

Throughout the field, an elastic-plastic behavior was observed. In terms of peak load, 40 µm Sized Surfaces, with an overall higher engineering stress range (85 – 195 MPa) prevails other lattice topologies, namely, Grass Hopper (25 – 100 MPa), Hexa Profile (35 – 70 MPa) and Penta Cube (45 – 125 MPa). In other words, peak load ranges have a direct correlation to the relative densities of the structures. Such a correlation has been reported by other researchers [6] when cell unit size and geometry are considered. Therefore, one of the advantages of lattice structures is that geometry features such as node spacing, strut thickness, orientation can be manipulated in order to control deformation behavior while experiencing external loads [7], [8]. It is worth noting the hardening-based stress behavior of some of the Penta Cube curves (20, 30 and 40 J/mm^2) show plateau and densification regions before structural fracture. This

phenomena could be caused by a multiplicity of factors, hence further analyses are required. Figure 16 illustrates the compressive flow stress curve behavior of the different ultra-fine lattice topologies as a function of varying the build energy density.

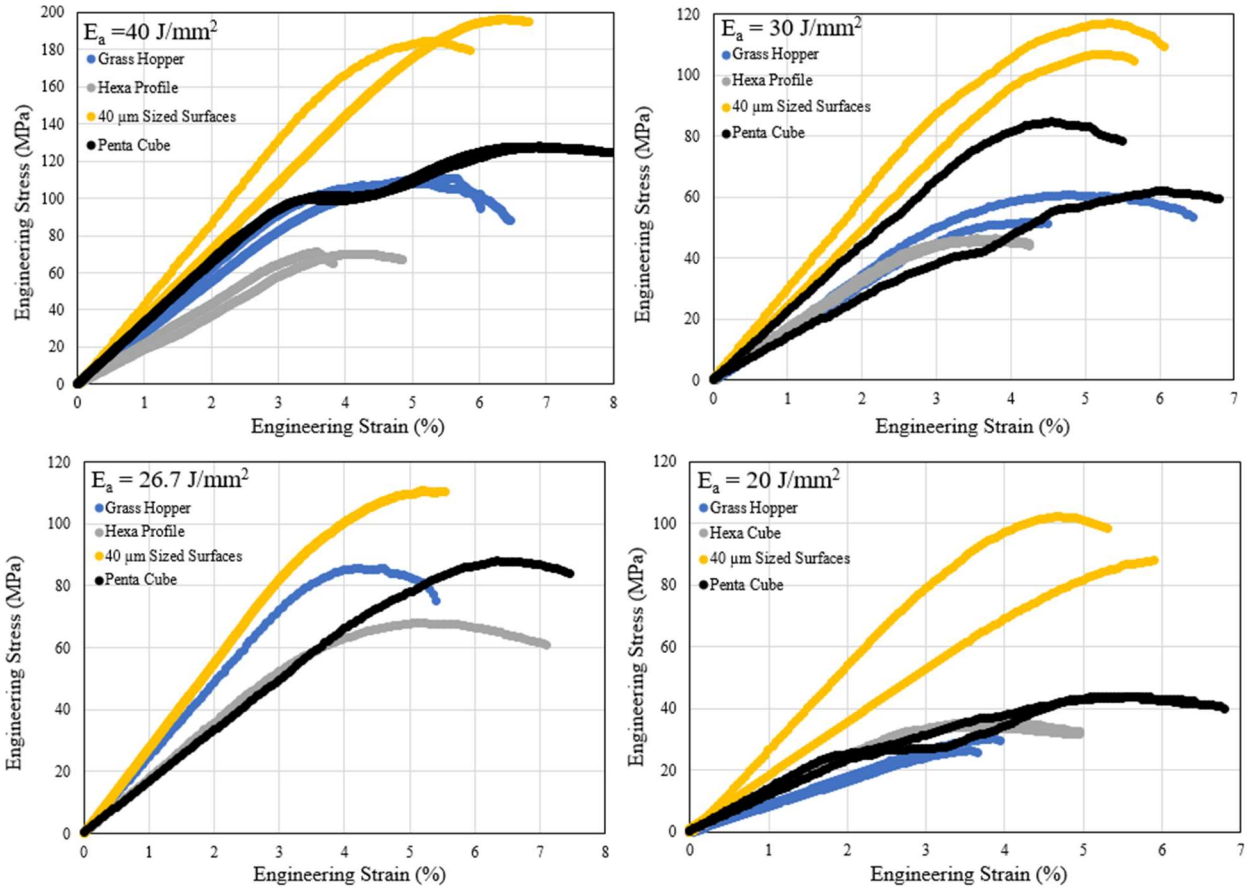

Fig. 16 Compressive strength of as-built AM W lattice structures with E_a is constant and topology is varied.

It can be observed that the 40 µm Sized Surfaces lattice topology consistently outperform the other lattice topologies. In addition, there is a direct correlation observed between the build energy density and the lattice peak load. This phenomena confirms what had been discussed previously in the microstructural characterization section, where a higher build energy density generates a larger melt pool, which when solidifies produces thicker struts that allow for a higher peak load to be withstood. Although a higher peak load for a given lattice topology at a specific energy density could be desirable as was observed from optical micrographs the corresponding pore size decreases inversely with energy density, directly impacting gas or liquid flow behavior.

Several of the compression tests were videoed to undergo digital image correlation that was used to extract ultra-fine lattice specimen deformation as a function of compression state. This evaluation method enables for the identification and refined understanding of how regional deformation moves throughout the lattice, from struts to nodes, as the load is increased during the compression test to failure. These results are then be used in subsequent structural analysis, which is beyond the scope of this documents. Ultimately, mechanical property data is used to baseline simulation and modeling tools to improve the lattice design process in order to optimize subsequent ultra-fine lattice topologies for expected load conditions.

At this point there is still insufficient information on which to be make an informed decision on what particular lattice topology and build parameter set are to be selected for use a specific propulsion catalyst application. Therefore, an additional selection criteria beyond geometric dimensions and mechanical behavior is required. In the following section we discuss characterization of gas and liquid flow through the different ultra-fine lattice topology types.

G. Flow Characterization

Pressure drop across a specimen measurements were conducted by the University of Texas at El Paso (UTEP) in order to determine flow through the lattice. The Flow Coefficient or K_v (m³/hour) is the relative efficiency of a restriction to allow fluid flow through it. K_v is defined as the amount of water that flows through a restriction at 16 °C with a pressure loss of 1 bar. K_v for water is calculated by equation (3).

$$K_v = Q\sqrt{\frac{\gamma}{\Delta P}} = \frac{Q}{\sqrt{\Delta P}} \tag{3}$$

Q is the volumetric flow rate (m³/hour), γ is the specific gravity of water (1 g/cm³) and ΔP is the pressure drop across the restriction (bar) [9]. Kv was also determined for subsonic ($\Delta P < \frac{P_1}{2}$) gaseous nitrogen using equation (4).

$$K_v = \frac{Q}{30.8 * \sqrt{\frac{\Delta P * P_2}{\gamma * T}}} \tag{4}$$

γ is the specific gravity (kg/m³) of the gas at standard conditions at 20 °C and T (K) is the gas absolute temperature [9]. One test apparatus for water and another for gaseous nitrogen were constructed, calibrated, and utilized to obtain the desired data. The gaseous apparatus is shown in Figure 17. Flow tests were conducted perpendicular to the build direction (XY) and parallel to the build direction (XZ) for both gaseous nitrogen and water.

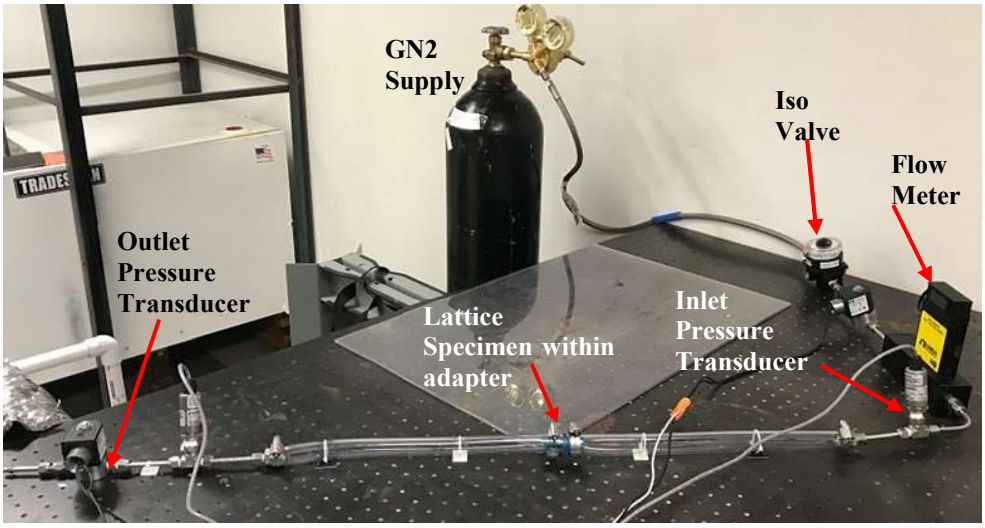

Fig. 17 Early version of gaseous nitrogen test apparatus.

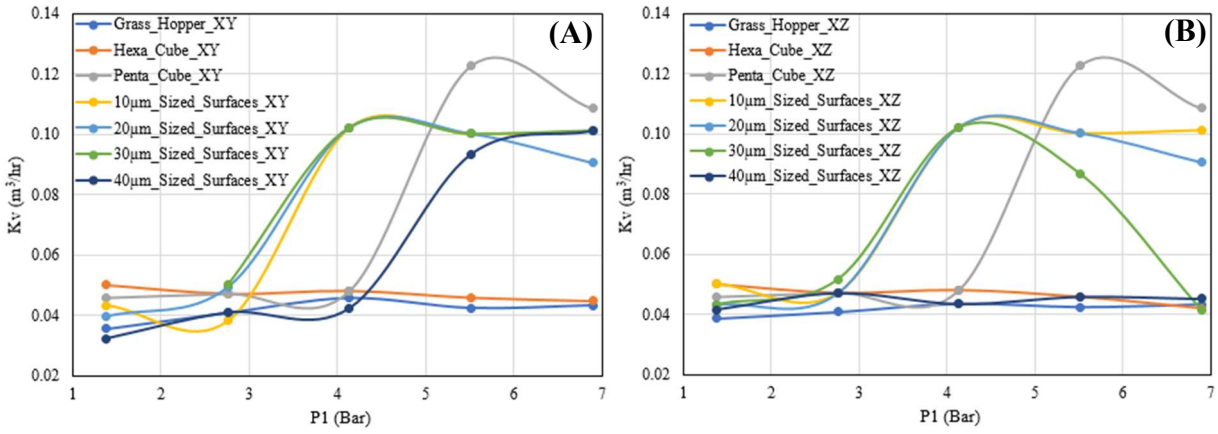

Fig. 18 K_v for water of Ti6Al4V lattice specimens in (A) XY and (B) XZ planes.

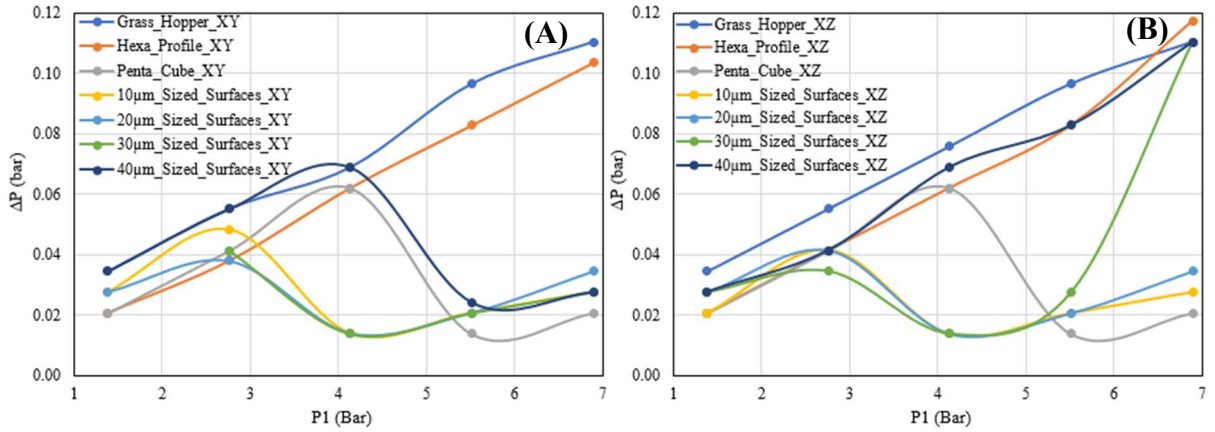

Fig. 19 *ΔP* for water of Ti6Al4V lattice specimens in (A) XY and (B) XZ planes

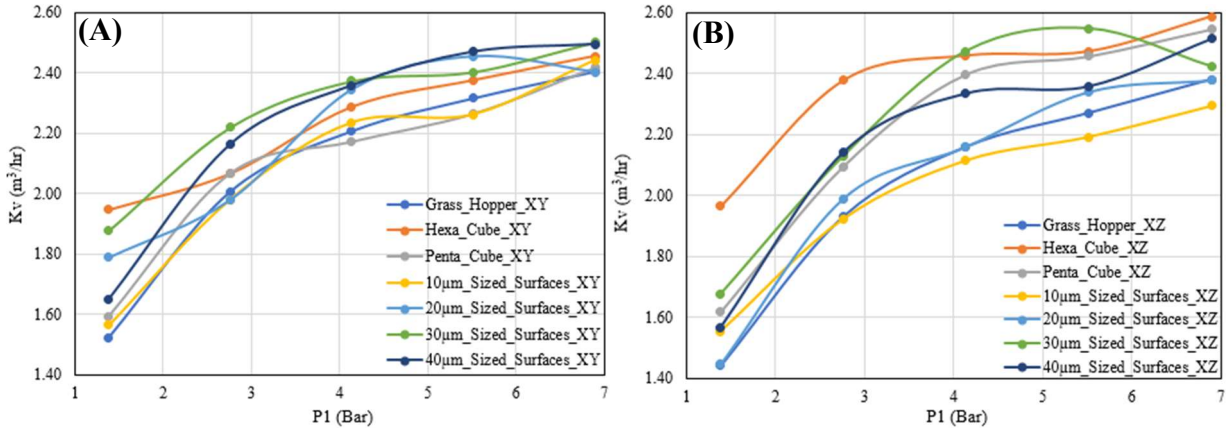

Fig. 20 K_v for GN2 of Ti6Al4V lattice specimens in (A) XY and (B) XZ planes.

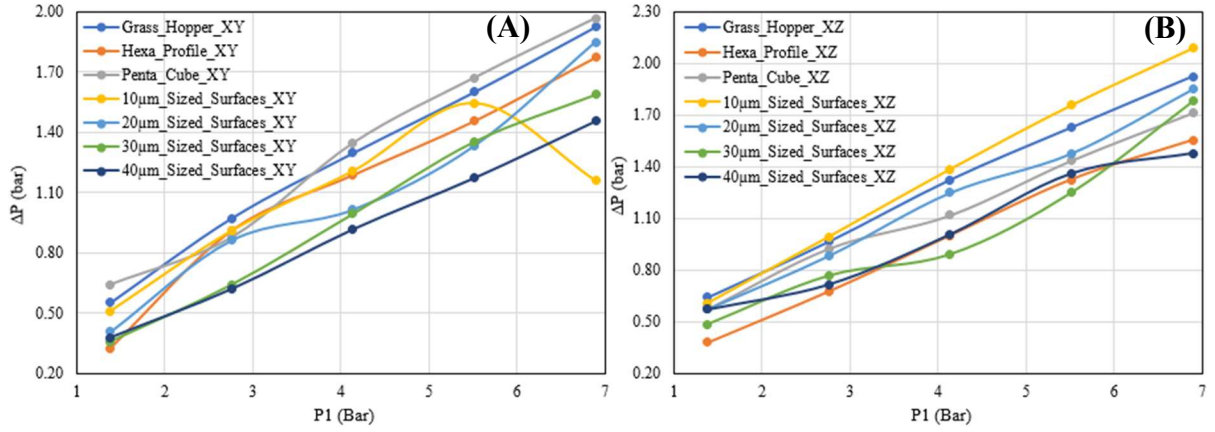

Fig. 21 ΔP for GN2 of Ti6Al4V lattice specimens in (A) XY and (B) XZ planes.

Results for gaseous nitrogen data show relatively consistent trends in K_v and ΔP as a function of both pressure and lattice topology. The water flow data has a larger degree of variability compared to the nitrogen results. No significant differences can be inferred between XY and XZ directions, with the dominant influence being lattice topology type. Previous studies have shown that the lattice unit cell has the largest influence on K_v and ΔP since a larger unit cell results in a larger pore diameter and more flow area [3]. For this specific application the small unit size is required to meet the operational intent and optimization of the unit cell size would likely yield little improvement in performance.

IV. Conclusion

AM ultra-fine lattices were not only shown to be viable but also met all requirements to as mono-propellant catalysts. Production costs in terms of feedstock, time, and post-processing is relatively low with improved schedule control. Seven lattice topologies were found to be functional for Ti6Al4V and four lattice topologies for W. Mechanical and flow properties were found to be as good or better over traditional coated foam products. Follow-on work includes lattice structure parameter development for a range of high temperature platinum catalytic metals to eliminate the need for a secondary coating process. Silver, rhodium, or iridium alloys are common catalytic elements, which are weldable metals and therefore suitable for L-PBF AM. Another L-PBF parameter development for iridium and post-processing process methods to yield ultra-fine lattice structures are in the planning stages. Methods for improved powder removal from lattice cell volume (i.e. ultrasonic or chemical) are also required. A more through characterization and modeling of flow properties for AM ultra-fine lattice structures should be conducted in order to compare to previous work on sintered metal porous media [10]. Ultimately, integration of AM lattice catalysts into AM refractory alloy thruster body and hot fire test campaign is necessary to increase the TRL for flight potential.

Acknowledgments

The authors would like to thank Daniel Cavender, Marvin Barnes, Trevor Bormann, and Jason Turpin of NASA MSFC; 3D Engineering Solutions; Edel Arrieta, Raul Cuevas, Pilar Gonzalez, Frank Medina, Jaclyn Mejia, and Jonathan Navarrete of UTEP; and Ankit Saharan of EOS North America. This project was funded under NASA Cooperative Agreement Notice #80MSFC19M0002.

References

[1] Cavender, D., et al., "*Design and Development of an Additively Manufactured 1N Green Propellant Thruster*," NASA T/M TBD – 2021.

[2] Shchetkovskiy, A and McKechnie, T., "*Development of Metallic Foam Monolithic Catalyst for Green Monopropellants Propulsion,*" Proceedings of the 2016 Space Propulsion Conference, Rome Italy, May 2016.

[3] Mireles, O.R., et al., "*Thermal, Fluid, Mechanical, and Microstructural Property Characterization of Additive Manufactured Lattice Structures*," Proceedings of the Additive Manufacture Technical Interchange Meeting, Huntsville AL, August 2018.

[4] Turner, J., *Atoms, Radiation, and Radiation Protection*, John Wiley & Sons Inc, New York, NY, 1995, pp. 187-192.

[5] Knoll, G. F., *Radiation Detection and Measurement* – 3th ed., John Wiley and Sons Inc., New York, NY, 1999, pp. 629-631.

[6] Hazeli, K., et al., "*Microstructure-Topology Relationship Effects on the Quasi-Static and Dynamic Behavior of Additively Manufactured Lattice Structures*," Materials and Design, Vol. 176, 2019.

[7] Pham, M. S., et al., "*Damage Tolerant Architected Materials Inspired by Crystal Microstructure*," Nature, Vol. 565, 2019, pp. 305-325.

[8] Zhao, S., et al., *"Compressive and Fatigue behavior of functionally graded Ti-6Al-4V meshes fabricated by electron beam melting,"* Acta Materialia, Vol. 150, 2018, pp. 1-15.

[9] Danfoss A/S, "Kv Technical Paper," 2019, http://heating.danfoss.com/PCMPDF/VFHBG202_kv.pdf

[10] Zhong, W., et al., "*Measurement and Determination of Friction Characteristic of Air Flow through Porous Media*," Metals, Vol. 5, 2015